Ultrahigh Doping of Graphene Using Flame-Deposited MoO_3

Sam Vaziri, *Member, IEEE*, Victoria Chen, Lili Cai, Yue Jiang, Michelle E. Chen, Ryan W. Grady, Xiaolin Zheng, and Eric Pop, *Senior Member, IEEE*

***Abstract*— The expected high performance of graphene-based electronics is often hindered by lack of adequate doping, which causes low carrier density and large sheet resistance. Many reported graphene doping schemes also suffer from instability or incompatibility with existing semiconductor processing. Here we report ultrahigh and stable *p*-type doping up to ~7×10^{13} cm^{-2} (~2×10^{21} cm^{-3}) of monolayer graphene grown by chemical vapor deposition. This is achieved by direct polycrystalline MoO_3 growth on graphene using a rapid flame synthesis technique. With this approach, the metal-graphene contact resistance for holes is reduced to ~200 $\Omega \cdot \mu$m. We also demonstrate that flame-deposited MoO_3 provides over 5× higher doping of graphene, as well as superior thermal and long-term stability, compared to electron-beam deposited MoO_3.**

***Index Terms*— Graphene, doping, contact resistance.**

I. Introduction

GRAPHENE is a two-dimensional (2D) material with unique physics and intrinsic properties [1]. This has resulted in many reports on proof-of-concept electronic and optoelectronic devices with functionalities that cannot be achieved by conventional bulk materials [2]–[4]. However, many such devices still suffer from issues such as low performance, poor reliability, device-to-device variation, and lack of reproducibility [5]–[7]. This partly occurs because atomically thin graphene (~0.335 nm monolayer) is very sensitive to perturbations introduced during or after its integration with other materials [8]. This high sensitivity also makes it challenging to achieve effective, reliable, and uniform doping of graphene without sacrificing its electronic quality [9]. As a result, applying conventional semiconductor doping methods (e.g. substituting C atoms with dopants) is very challenging for graphene and other 2D materials.

A more promising route to control the doping of graphene and other 2D materials is to introduce charge carriers from the outside, either with a field-effect (electrostatically or with external charge dipoles) or by external dopants (similar to modulation doping in conventional semiconductors) [10]–[13]. For example, charge transfer from external metal-oxide layers is one of the most promising mechanisms, being compatible with semiconductor device processing while minimally degrading the electronic properties of graphene [14], [15]. In this doping scheme, a metal-oxide with a different electron affinity is brought into contact with graphene, transferring charge carriers across the interface and forming interface dipoles. For example, *p*-type doping of graphene can be achieved by capping with molybdenum oxide (MoO_x where $x \sim 3$) with large electron affinity >6 eV [10]. MoO_3 also has a sufficiently large band gap ($E_G \sim 3.7$ eV) to be compatible with transparent electronic applications. However, due to varying material quality and measurement conditions, reported results have not been consistent [10], [15]–[17]. Thus, the effectiveness of graphene doping remains challenging, while little is known about long-term stability [13].

In this letter, we apply MoO_3 using a rapid flame vapor deposition technique [18] to effectively induce ultrahigh and stable *p*-type doping of graphene monolayers grown by chemical vapor deposition (CVD). We use electrical measurements, Raman spectroscopy, and modeling to show that a thin layer of ~5 nm flame-deposited MoO_3 on monolayer graphene can induce a hole density of ~7×10^{13} cm^{-2} and a metal-graphene contact resistance of ~200 $\Omega \cdot \mu$m. We compare the effectiveness of this method to the conventional approach of electron-beam (e-beam) evaporated MoO_3. The results are averaged over tens of test structures and show long-term stability.

II. Graphene Field-Effect Test Structures

Monolayer graphene was grown on Cu foil using CVD, and subsequently transferred [19] onto 90 nm SiO_2 on p^+ Si substrates which also serve as back-gates. After defining graphene channels by photolithography and oxygen plasma, 50 nm-thick Pd contacts were formed using e-beam lithography, e-beam deposition, and lift-off. Similar steps were repeated to form Ti(3 nm)/Au(70 nm) electrical contact pads. Figure 1(a) shows a representative transfer length method (TLM) test device with 8 channel lengths, 500 nm $\leq L \leq$ 22 μm. Then, the

Manuscript received July 24, 2020; revised August 11, 2020; accepted August 18, 2020. Date of publication August 21, 2020; date of current version September 25, 2020. This work was supported by Bosch through the Stanford SystemX Alliance. The work of Sam Vaziri was supported by the Knut and Alice Wallenberg Foundation Fellowship. The work of Ryan W. Grady was supported by the NSF Graduate Research Fellowship Program (GRFP) under Grant DGE-1656518. The review of this letter was arranged by Editor D. Shahrjerdi. *(Corresponding author: Eric Pop.)*

Sam Vaziri, Victoria Chen, and Ryan W. Grady are with the Department of Electrical Engineering, Stanford University, Stanford, CA 94305 USA.

Lili Cai, Yue Jiang, and Xiaolin Zheng are with the Department of Mechanical Engineering, Stanford University, Stanford, CA 94305 USA.

Michelle E. Chen is with the Department of Materials Science and Engineering, Stanford University, Stanford, CA 94305 USA.

Eric Pop is with the Department of Electrical Engineering, Stanford University, Stanford, CA 94305 USA, and also with the Department of Materials Science and Engineering, Stanford University, Stanford, CA 94305 USA (e-mail: epop@stanford.edu).

Color versions of one or more of the figures in this letter are available online at http://ieeexplore.ieee.org.

Digital Object Identifier 10.1109/LED.2020.3018485

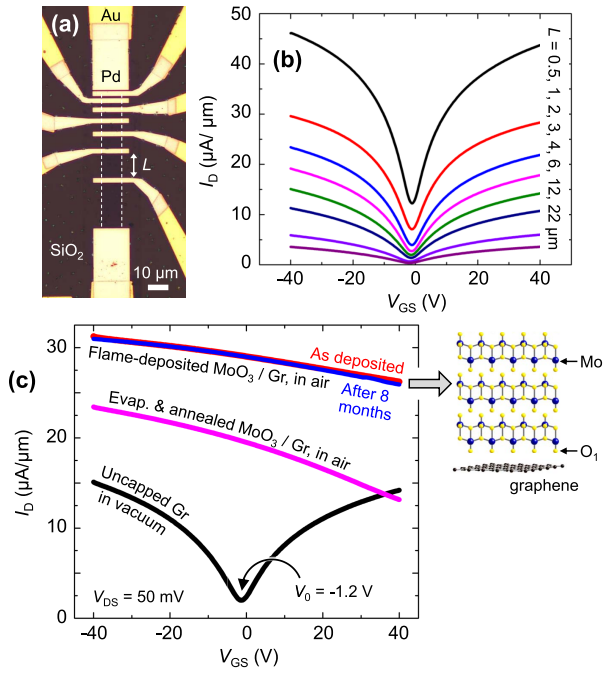

Fig. 1. **Transfer characteristics at room temperature. (a)** Optical image of a TLM test structure with channel lengths of 0.5 μm, 1 μm, 2 μm, 3 μm, 4 μm, 6 μm, 12 μm and 22 μm. **(b)** Measured current (I_D) vs. gate voltage (V_{GS}) of uncapped graphene channels in the TLM. **(c)** Measured I_D-V_{GS} of a graphene (Gr) channel with $L = 4$ μm: uncapped (black line), capped with evaporated (magenta line) and flame deposited (red line) MoO_3. The blue line shows the same device as in red, after 8 months. The schematic shows the crystalline MoO_3 interface with graphene.

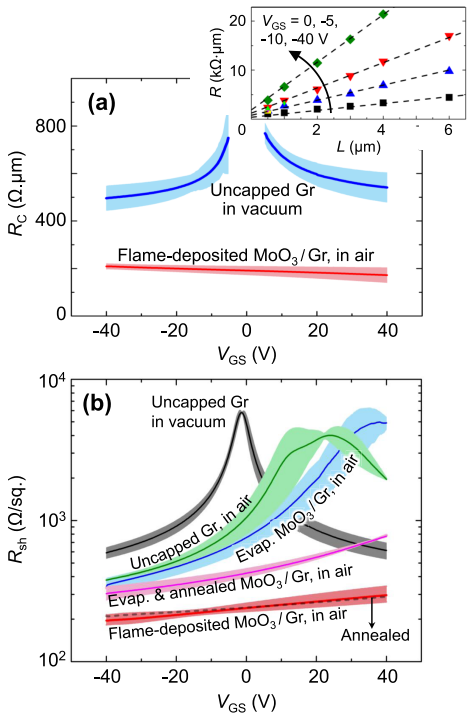

Fig. 2. **Contact and sheet resistance from TLM. (a)** Pd-graphene (Gr) contact resistance R_C vs. V_{GS} with Gr channel uncapped (blue) and capped with flame-grown MoO_3 (red). Inset shows TLM plot and fitting (dashed lines). **(b)** Extracted graphene sheet resistance for uncapped and capped graphene channels before and after annealing. Solid lines show the average resistance and the shaded regions put bounds on the maximum and minimum values over all the measured TLMs. Black dashes show the average sheet resistance of the flame-deposited MoO_3 after annealing.

samples were annealed at 250°C in vacuum (5×10^{-5} Torr). Figure 1(b) shows the transfer characteristics of the back-gated graphene field effect transistors (GFETs) making up the TLM in vacuum. These display very symmetric ambipolar behavior with Dirac voltage (V_0) near zero and minimal hysteresis, indicating clean, nearly intrinsic graphene channels.

In previous work [18] we showed that atomically thin MoO_3 can be grown on layered materials such as WSe_2 and graphene, using flame synthesis by van der Waals epitaxy. Unlike e-beam evaporation, the flame-deposited MoO_3 on layered materials shows a high degree of crystallinity. Here, we use this method to deposit thin layers (~5 to 10 nm) of MoO_3 on the graphene channels to induce strong p-type doping.

Figure 1(c) shows measurements of an uncapped GFET in vacuum (black line) which exhibits a maximum hole mobility ~2700 $cm^2V^{-1}s^{-1}$ and an on/off current ratio of ~7.5 with a hysteresis $|\Delta V_0| \approx 0.5$ V (not shown). After the flame deposition of MoO_3, the transfer characteristics of the same device show a significant positive shift of the Dirac voltage (beyond the V_{GS} range we can apply safely without damaging the back-gate oxide), indicative of strong p-type doping [Fig. 1(c), red line].

Importantly, re-measuring the same device after 8 months [Fig. 1(c), blue line] shows no significant variation or degradation in the drain current, indicating excellent long-term stability. We attribute this stability to the high crystallinity and stoichiometry of the flame-deposited MoO_3 on graphene [18]. For comparison, e-beam evaporated MoO_3 was applied on separate samples, which were then annealed in air at 200 °C for 30 min. The effect of annealing is discussed in the next section. For the same channel length of 4 μm, the GFET capped with the evaporated MoO_3 [Fig. 1(c), magenta curve] has lower drain current than GFETs capped with the flame-deposited MoO_3.

III. Sheet and Contact Resistance

After process development, we performed six MoO_3 flame depositions and two MoO_3 evaporation runs. Then we characterized on average twelve TLM structures [20] for each deposition run, with Fig. 2 showing extracted contact resistance R_C and sheet resistance R_{sh} for the uncapped and MoO_3-capped samples. The inset shows the TLM plot of resistance vs. length for uncapped devices. In Fig. 2(a), the uncapped devices (blue line) show relatively symmetric Pd-graphene contacts for electrons and holes, suggesting Fermi level pinning near the Dirac point. When approaching the Dirac voltage, R_C increases as the graphene density of states decreases. For holes in doped graphene (red line), we note $R_C \sim 200\ \Omega \cdot \mu$m at room temperature, which improves at least by a factor of 2.5 the lowest R_C achieved in the uncapped devices. This contact resistance is comparable to the lowest reported values for Pd with exfoliated monolayer graphene [21].

Figure 2(b) shows the extracted R_{sh} from TLMs for all the uncapped and capped graphene channels before and after annealing. Interestingly, while the annealing changes the doping of graphene capped with evaporated MoO_x [Fig. 2(b), blue and magenta lines], it does not affect the graphene

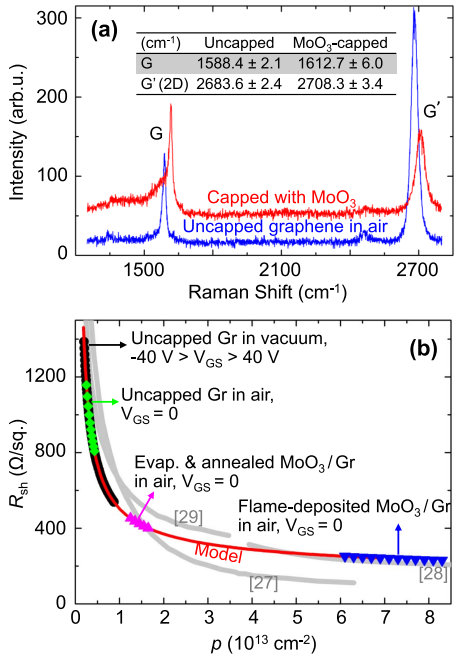

Fig. 3. **Raman analysis and charge carrier extraction. (a)** Raman spectra of the uncapped and capped with flame-deposited MoO_3 graphene in air. The inset table shows the average (15 spots each) G and G' peak positions before and after MoO_3 deposition. **(b)** Data fitting to the model and carrier density extraction for capped devices. Gray lines show experimental data from Refs. [27]–[29], for comparison.

capped with flame-deposited MoO_3 [Fig. 2(b), black dashed line]. This shows that the flame-deposited MoO_3 is thermally more stable than the evaporated one due to its stoichiometric and crystalline characteristics [18]. Figure 2(b) shows that while electrostatic gating can reduce uncapped graphene sheet resistance by about one order of magnitude, the MoO_3 can further and significantly dope graphene, even beyond the electrostatic gating limit. While the large ranges for uncapped samples and those capped with evaporated MoO_3 are due to larger hysteresis and device-to-device variation, the annealed graphene devices capped with flame-deposited MoO_3 show significantly lower variation.

We attribute the higher doping to two underlying causes. The flame deposition method generates highly crystalline, stoichiometric MoO_3, with more terminal O_1 sites that create a dipole layer to increase its work function [18], [22]. In addition, flame-deposited MoO_3 is horizontally oriented with the (010) planes parallel to the graphene basal plane [Fig. 1(c)]. Because the terminal O_1 sites are located on the (010) plane, this orientation creates a stronger dipole layer on the surface, which enables higher charge transfer doping of graphene. In contrast, thermal evaporation generates amorphous, sub-stoichiometric and randomly oriented MoO_x ($x < 3$).

Using Raman spectroscopy, we further monitored the carrier density through the G and G' (also known as 2D) peaks [23]. Figure 3(a) shows the Raman spectra of graphene before (blue line) and after (red line) the flame deposition of MoO_3, measured in air. No significant disorder-related D peak (at 1350 cm^{-1}) indicates good quality of graphene even after MoO_3 deposition. The capped graphene shows a significant blue shift of G and G' (2D) peaks from

TABLE I
SHEET RESISTANCE, CHARGE CARRIER DENSITY, AND RESISTANCE RATIO AVERAGED OVER ALL THE MEASURED GRAPHENE DEVICES

	R_{sh} (Ω/sq.)	p (cm^{-2})	R/R_0 (vac.)	R/R_0 (air)
Gr in vac.	5700	-	-	-
Gr in air	980	3.4×10^{12}	17%	-
Gr / evap. MoO_3	423	1.4×10^{13}	7%	43%
Gr / flame MoO_3	230	7.2×10^{13}	4%	23%

~1588.4 cm^{-1} to ~1612.7 cm^{-1}, and from ~2683.6 cm^{-1} to ~2708.3 cm^{-1}, respectively [inset of Fig. 3(a)]. The G' peak of the capped graphene in Fig. 3(a) exhibits substantial intensity drop and line broadening, which are mainly ascribed to the large hole doping [23]. Comparing these peak shifts and the intensity ratio of G and G' peaks for the capped graphene [I(G')/I(G) < 0.77] to the electrochemical-gate calibrated graphene in Ref. [23] suggests p-doping $>3\times10^{13}cm^{-2}$ in the graphene capped with flame-deposited MoO_3. However, we note that the possible strain effect of the capping layer can contribute to the peak shifts and variations affecting the accuracy of the doping estimate from the Raman spectra.

Because the Dirac voltage is outside the measurable V_{GS} range for the capped devices, it is not possible to directly extract the carrier density from the measured I_D vs. V_{GS}. Hence, we applied a well-tested model [24], [25] to estimate the carrier density in the graphene channels from our electrical results. This model is based on the power law behavior of mobility *vs.* carrier concentration $\mu(p) \propto p^{-\alpha}$ [26]. We fit our uncapped graphene data [Fig. 3(b), thick black line] as $R_{sh} = [1 + (p/p_{ref})^{\alpha}]/(qp\mu_0)$, shown with the red line, where $\mu_0 = 3350\ cm^2V^{-1}s^{-1}$, $p_{ref} = 5.14\times10^{12}\ cm^{-2}$, and $\alpha = 0.8$. R_{sh}, p and q are sheet resistance, hole density, and elementary charge, respectively. Then the carrier densities in the capped devices with evaporated [magenta symbols in Fig. 3(b)] and flame-deposited MoO_3 [blue symbols in Fig. 3(b)] are extracted. For comparison, the gray lines in Fig. 3(b) show experimental data from previous Hall measurements at high carrier densities achieved by electrolyte gating [27], [28] and nitric acid doping [29], demonstrating similar behavior. Table I summarizes our average sheet resistance, estimated carrier densities, and the resistance ratio (R/R_0) at zero gate voltage, where R_0 and R are the resistances of uncapped and capped-with-MoO_3 graphene channels, respectively.

IV. CONCLUSION

In conclusion, we applied our flame vapor deposition technique to grow thin films of stoichiometric crystalline MoO_3 on monolayer CVD graphene. The resulting structures exhibit an ultrahigh and stable p-type charge transfer doping up to ~7×10^{13} cm^{-2}, five times higher than control samples with e-beam evaporated MoO_3. Using this approach, the metal (Pd)-graphene contact resistance was also reduced by a factor of 2.5 to ~200 $\Omega\cdot\mu m$. Our fabrication process is CMOS-compatible and can be used to realize competitive performance in graphene electronics, as well as low-sheet-resistance transparent conductors.

REFERENCES

[1] A. K. Geim and K. S. Novoselov, "The rise of graphene," *Nature Mater.*, vol. 6, no. 3, pp. 183–191, Mar. 2007, doi: 10.1038/nmat1849.

[2] C.-H. Liu, Y.-C. Chang, T. B. Norris, and Z. Zhong, "Graphene photodetectors with ultra-broadband and high responsivity at room temperature," *Nature Nanotechnol.*, vol. 9, no. 4, pp. 273–278, Mar. 2014, doi: 10.1038/nnano.2014.31.

[3] L. Britnell, R. V. Gorbachev, R. Jalil, B. D. Belle, F. Schedin, A. Mishchenko, T. Georgiou, M. I. Katsnelson, L. Eaves, S. V. Morozov, N. M. R. Peres, J. Leist, A. K. Geim, K. S. Novoselov, and L. A. Ponomarenko, "Field-effect tunneling transistor based on vertical graphene heterostructures," *Science*, vol. 335, no. 6071, pp. 947–950, Feb. 2012, doi: 10.1126/science.1218461.

[4] S. Vaziri, G. Lupina, C. Henkel, A. D. Smith, M. Östling, J. Dabrowski, G. Lippert, W. Mehr, and M. C. Lemme, "A graphene-based hot electron transistor," *Nano Lett.*, vol. 13, no. 4, pp. 1435–1439, Mar. 2013, doi: 10.1021/nl304305x.

[5] G. Xu, Y. Zhang, X. Duan, A. A. Balandin, and K. L. Wang, "Variability effects in graphene: Challenges and opportunities for device engineering and applications," *Proc. IEEE*, vol. 101, no. 7, pp. 1670–1688, Jul. 2013, doi: 10.1109/JPROC.2013.2247971.

[6] S. Vaziri, A. D. Smith, M. Östling, G. Lupina, J. Dabrowski, G. Lippert, W. Mehr, F. Driussi, S. Venica, V. Di Lecce, A. Gnudi, M. König, G. Ruhl, M. Belete, and M. C. Lemme, "Going ballistic: Graphene hot electron transistors," *Solid State Commun.*, vol. 224, pp. 64–75, Dec. 2015, doi: 10.1016/j.ssc.2015.08.012.

[7] A. D. Smith, S. Wagner, S. Kataria, B. G. Malm, M. C. Lemme, and M. Ostling, "Wafer-scale statistical analysis of graphene field-effect transistors—Part II: Analysis of device properties," *IEEE Trans. Electron Devices*, vol. 64, no. 9, pp. 3927–3933, Sep. 2017, doi: 10.1109/TED.2017.2727823.

[8] A. D. Smith, K. Elgammal, F. Niklaus, A. Delin, A. C. Fischer, S. Vaziri, F. Forsberg, M. Råsander, H. Hugosson, L. Bergqvist, S. Schröder, S. Kataria, M. Östling, and M. C. Lemme, "Resistive graphene humidity sensors with rapid and direct electrical readout," *Nanoscale*, vol. 7, no. 45, pp. 19099–19109, 2015, doi: 10.1039/c5nr06038a.

[9] D. Wei, Y. Liu, Y. Wang, H. Zhang, L. Huang, and G. Yu, "Synthesis of N-doped graphene by chemical vapor deposition and its electrical properties," *Nano Lett.*, vol. 9, no. 5, pp. 1752–1758, May 2009, doi: 10.1021/nl803279t.

[10] S. Chandramohan, T. H. Seo, V. Janardhanam, C.-H. Hong, and E.-K. Suh, "A comparison of various surface charge transfer hole doping of graphene grown by chemical vapour deposition," *Appl. Surf. Sci.*, vol. 418, pp. 258–263, Oct. 2017, doi: 10.1016/j.apsusc.2017.01.097.

[11] K. Kanahashi, N. Tanaka, Y. Shoji, M. Maruyama, I. Jeon, K. Kawahara, M. Ishihara, M. Hasegawa, H. Ohta, H. Ago, Y. Matsuo, S. Okada, T. Fukushima, and T. Takenobu, "Formation of environmentally stable hole-doped graphene films with instantaneous and high-density carrier doping via a boron-based oxidant," *npj 2D Mater. Appl.*, vol. 3, no. 1, p. 7, Feb. 2019, doi: 10.1038/s41699-019-0090-x.

[12] A. Kasry, M. A. Kuroda, G. J. Martyna, G. S. Tulevski, and A. A. Bol, "Chemical doping of large-area stacked graphene films for use as transparent, conducting electrodes," *ACS Nano*, vol. 4, no. 7, pp. 3839–3844, Jul. 2010, doi: 10.1021/nn100508g.

[13] A. N. Mehta, W. Mu, M. Murugesan, Y. Jiao, Y. Fu, P. Hyldgaard, and J. Liu, "Understanding noninvasive charge transfer doping of graphene: A comparative study," *J. Mater. Sci., Mater. Electron.*, vol. 29, no. 7, pp. 5239–5252, Apr. 2018, doi: 10.1007/s10854-017-8443-8.

[14] J. Meyer, P. R. Kidambi, B. C. Bayer, C. Weijtens, A. Kuhn, A. Centeno, A. Pesquera, A. Zurutuza, J. Robertson, and S. Hofmann, "Metal oxide induced charge transfer doping and band alignment of graphene electrodes for efficient organic light emitting diodes," *Sci. Rep.*, vol. 4, no. 1, p. 5380, Jun. 2014, doi: 10.1038/srep05380.

[15] S. Kim, S. Shin, T. Kim, H. Du, M. Song, K. S. Kim, S. Cho, S. W. Lee, and S. Seo, "A reliable and controllable graphene doping method compatible with current CMOS technology and the demonstration of its device applications," *Nanotechnology*, vol. 28, no. 17, Apr. 2017, Art. no. 175710, doi: 10.1088/1361-6528/aa6537.

[16] L. D'Arsié, S. Esconjauregui, R. Weatherup, Y. Guo, S. Bhardwaj, A. Centeno, A. Zurutuza, C. Cepek, and J. Robertson, "Stability of graphene doping with MoO_3 and I_2," *Appl. Phys. Lett.*, vol. 105, no. 10, Sep. 2014, Art. no. 103103, doi: 10.1063/1.4895025.

[17] Q.-H. Wu, Y. Zhao, G. Hong, J.-G. Ren, C. Wang, W. Zhang, and S.-T. Lee, "Electronic structure of MoO_{3-x}/graphene interface," *Carbon*, vol. 65, pp. 46–52, Dec. 2013, doi: 10.1016/j.carbon.2013.07.091.

[18] L. Cai, C. J. McClellan, A. L. Koh, H. Li, E. Yalon, E. Pop, and X. Zheng, "Rapid flame synthesis of atomically thin MoO_3 down to monolayer thickness for effective hole doping of WSe_2," *Nano Lett.*, vol. 17, no. 6, pp. 3854–3861, Jun. 2017, doi: 10.1021/acs.nanolett.7b01322.

[19] S. Vaziri, E. Yalon, M. Muñoz Rojo, S. V. Suryavanshi, H. Zhang, C. J. McClellan, C. S. Bailey, K. K. H. Smithe, A. J. Gabourie, V. Chen, S. Deshmukh, L. Bendersky, A. V. Davydov, and E. Pop, "Ultrahigh thermal isolation across heterogeneously layered two-dimensional materials," *Sci. Adv.*, vol. 5, no. 8, Aug. 2019, Art. no. eaax1325, doi: 10.1126/sciadv.aax1325.

[20] S. Venica, F. Driussi, A. Gahoi, P. Palestri, M. C. Lemme, and L. Selmi, "On the adequacy of the transmission line model to describe the graphene–metal contact resistance," *IEEE Trans. Electron Devices*, vol. 65, no. 4, pp. 1589–1596, Apr. 2018, doi: 10.1109/TED.2018.2802946.

[21] F. Xia, V. Perebeinos, Y. M. Lin, Y. Wu, and P. Avouris, "The origins and limits of metal-graphene junction resistance," *Nature Nanotechnol.*, vol. 6, no. 3, pp. 179–184, Mar. 2011, doi: 10.1038/nnano.2011.6.

[22] Y. Guo and J. Robertson, "Origin of the high work function and high conductivity of MoO3," *Appl. Phys. Lett.*, vol. 105, no. 22, Dec. 2014, Art. no. 222110, doi: 10.1063/1.4903538.

[23] A. Das, S. Pisana, B. Chakraborty, S. Piscanec, S. K. Saha, U. V. Waghmare, K. S. Novoselov, H. R. Krishnamurthy, A. K. Geim, A. C. Ferrari, and A. K. Sood, "Monitoring dopants by Raman scattering in an electrochemically top-gated graphene transistor," *Nature Nanotechnol.*, vol. 3, no. 4, pp. 210–215, Apr. 2008, doi: 10.1038/nnano.2008.67.

[24] W. Zhu, V. Perebeinos, M. Freitag, and P. Avouris, "Carrier scattering, mobilities, and electrostatic potential in monolayer, bilayer, and trilayer graphene," *Phys. Rev. B, Condens. Matter*, vol. 80, no. 23, Dec. 2009, Art. no. 235402, doi: 10.1103/PhysRevB.80.235402.

[25] V. E. Dorgan, M. H. Bae, and E. Pop, "Mobility and saturation velocity in graphene on SiO_2," *Appl. Phys. Lett.*, vol. 97, no. 8, Aug. 2010, Art. no. 0821112, doi: 10.1063/1.3483130.

[26] A. Konar, T. Fang, and D. Jena, "Effect of high-k gate dielectrics on charge transport in graphene-based field effect transistors," *Phys. Rev. B, Condens. Matter*, vol. 82, no. 11, Sep. 2010, Art. no. 115452, doi: 10.1103/PhysRevB.82.115452.

[27] D. K. Efetov and P. Kim, "Controlling electron-phonon interactions in graphene at ultrahigh carrier densities," *Phys. Rev. Lett.*, vol. 105, no. 25, Dec. 2010, Art. no. 256805, doi: 10.1103/PhysRevLett.105.256805.

[28] J. Zhao, M. Wang, H. Li, X. Zhang, L. You, S. Qiao, B. Gao, X. Xie, and M. Jiang, "Lithium-ion-based solid electrolyte tuning of the carrier density in graphene," *Sci. Rep.*, vol. 6, no. 1, p. 34816, Oct. 2016, doi: 10.1038/srep34816.

[29] J. B. Bult, R. Crisp, C. L. Perkins, and J. L. Blackburn, "Role of dopants in long-range charge carrier transport for p-type and n-type graphene transparent conducting thin films," *ACS Nano*, vol. 7, no. 8, pp. 7251–7261, Jul. 2013, doi: 10.1021/nn402673z.